Influence of Inverter Controller Parameters on the Small-signal Stability of LCC-HVDC System Based on a Practical Project

Huan LI[1]* and Kang QIN[1]

[1]Electrical Power Research Institute, CSG, State Key Laboratory of HVDC. Guangzhou, China

Abstract. Unreasonable control parameters of the Line Commutated Converter based High Voltage Direct Current (LCC-HVDC) system may induce small-signal instability. This paper studies the impact of inverter controller parameters on steady response of the LCC-HVDC system under weak AC grid condition. Firstly, according to a practical project, the small-signal model of LCC-HVDC system is established based on the switching function. Then, the eigen-analysis method is adopted to study the impact of the controller parameters on the inverter side on the oscillation mode and damping characteristics of the LCC system, and the correctness of results is verified by PSCAD/EMTDC simulation. The conclusion shows that reasonable controller parameters can improve the stability margin of the system.

1 Introduction

Line Commutated Converter based High Voltage Direct Current (LCC-HVDC) system has the advantages of lower loss and large capacity power transmission, which plays an important role in realizing the optimal configuration of cross-regional power resources [1]. However, when the inverter station is connected to a weak grid, some inherent problems of LCC-HVDC system may arise such as commutation failure and voltage instability issues. The occurrence of these problems is largely affected by control parameters of the system [2],[3].

References [4]-[6] analyze the effects of the phase-locked loop (PLL) parameters and AC system parameters on the steady performance of LCC-HVDC system. The results show that the stability of LCC rectifier station is enhanced with the increase of PLL parameters, while the conclusion for the inverter station is just the opposite. In [7]-[8], the impact of PLL and constant extinction angle control parameters on the stability of the system is investigated based on a linearized dynamic model of the LCC inverter station. However, the rectifier station and DC line are equivalent to an ideal current source, so the influence of short circuit ratio (SCR) on the rectifier side on the stability of the system is ignored. In [9]-[10], a comprehensive comparison of the impact of constant voltage control and constant extinction angle control on small-signal stability of HVDC is conducted, and the stable region of control parameters which can maintain the stable operation of system is calculated. In the aspect of the small-signal analysis, the existing literatures are based on the CIGRE benchmark model [11] to study the influence of control parameters. However, the structure of AC/DC filter banks applied in the practical engineering is more complex, so there is a need to take a practical LCC-HVDC system as the studied object and analyze how to choose controller parameters reasonably to enhance the small-signal stability of the system.

The rest of this paper is organized as follows. In Section 2, a dynamic phasor model of LCC-HVDC system on basis of a practical project is established. The correctness of the small-signal model is verified by PSCAD/EMTDC simulation in Section 3. Section 4 presents the impact of controller parameters at the inverter station on small-signal stability of the system under weak AC grid condition by adopting eigenvalue analysis. Finally, Section 5 concludes the paper.

2 Small-signal dynamic model

2.1. Study system

The study system is a monopole double-ended 12-pulse LCC-HVDC system which is based on a practical engineering. Constant current control strategy is adopted at the rectifier station while constant voltage control strategy is used at the inverter station. The single-line diagram of the system is shown in figure 1. The subscript r and i represent the variables on the rectifier side and the inverter side, respectively. V_s denotes the AC system voltage. U_{pcc} represents the line voltage at the point of common coupling (PCC). i_s and i_c are the current of AC system and the converter transformer, respectively. The DC transmission line is equivalent to the T-type circuit. R_{dc} and L_{dc} represent resistance and inductance of DC line. L_{ec} is the sum of the equivalent inductance of the converter on the DC side and the inductance of the smoothing reactor. Additionally, L_T is the equivalent inductance of the transformer. R_s and L_s denote resistance and inductance of AC system. Z_{fac} and Z_{fdc} represent AC filter banks and DC

*Corresponding author's e-mail: lihuan3@csg.cn

filter banks, the specific configurations of which are shown in figure 2 and figure 3, respectively.

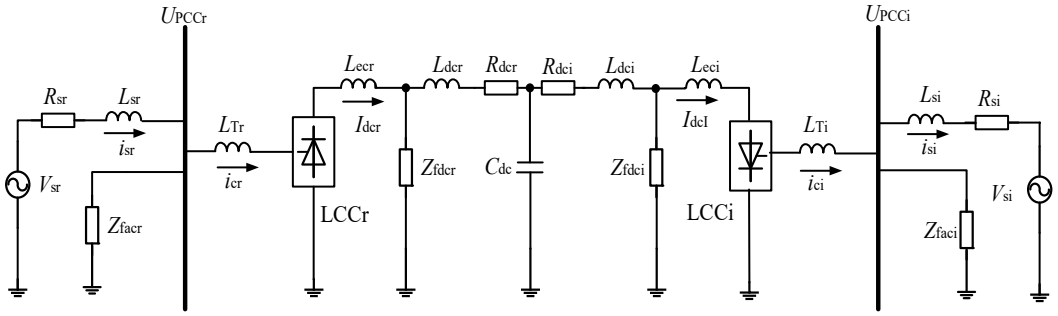

Figure 1. Single-line diagram of the LCC-HVDC system.

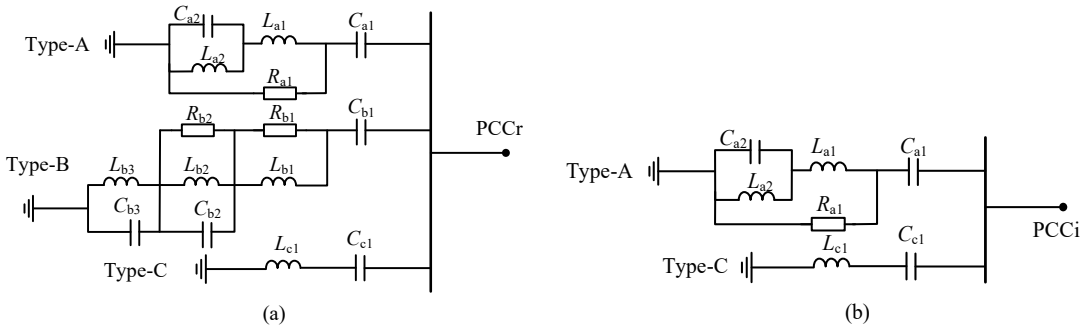

Figure 2. The configuration of the AC filter banks: (a) the rectifier side; (b) the inverter side.

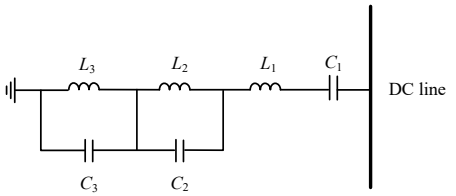

Figure 3. The configuration of the DC filter banks.

2.2. State space model

2.2.1 Converter station model. In this paper, the switching function method is used to describe the input/output relationship of converter station [9]. Take the rectifier station as an example. The AC side current of converter can be derived as

$$\begin{cases} i_{\mathrm{cdr}} = 2I_{\mathrm{dcr}}A_{\mathrm{i}}\cos(\varphi_{\mathrm{r}} + \theta_{\mathrm{PLLr}} - \omega_0 t - \theta_{\mathrm{acr0}}) \\ i_{\mathrm{cqr}} = -2I_{\mathrm{dcr}}A_{\mathrm{i}}\sin(\varphi_{\mathrm{r}} + \theta_{\mathrm{PLLr}} - \omega_0 t - \theta_{\mathrm{acr0}}) \end{cases} \quad (1)$$

where

$$A_{\mathrm{i}} = \frac{2\sqrt{3}}{\pi}\frac{\sin\dfrac{\mu_{\mathrm{r}}}{2}}{\dfrac{\mu_{\mathrm{r}}}{2}} \quad (2)$$

In (1), i_{cdr} and i_{cqr} are d-axis and q-axis component of the AC side current of converter. I_{dcr} is DC side current and φ_{r} is power factor angle. θ_{PLLr} is the output angle from PLL while θ_{acr0} is the initial phase of the voltage of PCC. ω_0 is the fundamental angular frequency. In (2), μ_{r} is commutation overlap angle.

2.2.2 The control system model. The block diagrams of the constant current controller and the constant voltage controller are shown in figure 4.

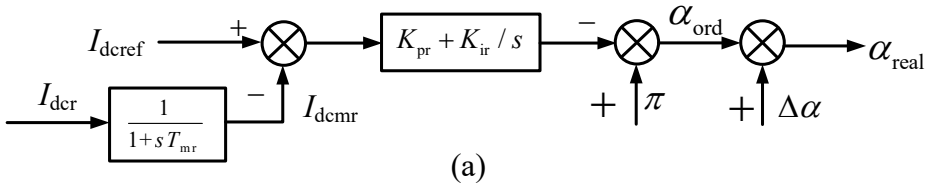

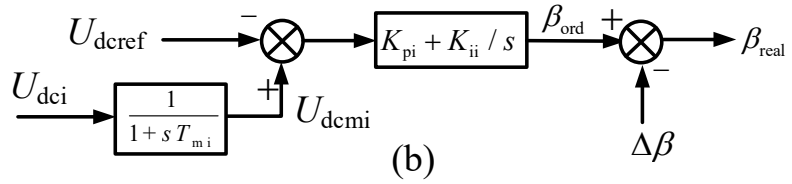

Figure 4. The block diagrams: (a) the constant current controller on the rectifier side; (b) the constant voltage controller on the inverter side.

The corresponding state space equation can be expressed as

$$\begin{cases} \dfrac{\mathrm{d}x_{1\mathrm{r}}}{\mathrm{d}t} = I_{\mathrm{dcref}} - I_{\mathrm{dcmr}} \\ \pi - \alpha_{\mathrm{ord}} = K_{\mathrm{pr}} \dfrac{\mathrm{d}x_{1\mathrm{r}}}{\mathrm{d}t} + K_{\mathrm{ir}} x_{1\mathrm{r}} \end{cases} \tag{3}$$

Where $x_{1\mathrm{r}}$ is the state variable of constant current controller and I_{dcref} is the reference DC-current. K_{pr} and K_{ir} are the proportion and the integral gain of the controller. The measured current I_{dcmr} is obtained by the actual DC current of rectifier through the first-order inertia link, whose state space equation can be expressed as

$$T_{\mathrm{mr}} \frac{\mathrm{d}I_{\mathrm{dcmr}}}{\mathrm{d}t} = I_{\mathrm{dcr}} - I_{\mathrm{dcmr}} \tag{4}$$

Where T_{mr} is the time constant of the first-order inertia link.

When the output angle of PLL (θ_{PLLr}) is not equal to the AC voltage phase of PCC (θ_{r}), there is a deviation $\Delta\alpha$ between the actual delay trigger angle α_{real} and the output reference angle α_{ord}. The expression is as follows:

$$\alpha_{\mathrm{real}} = \alpha_{\mathrm{ord}} + (\theta_{\mathrm{r}} - \theta_{\mathrm{PLLr}}) = \alpha_{\mathrm{ord}} + (\omega_0 t + \theta_{\mathrm{acr0}} - \theta_{\mathrm{PLLr}}) = \alpha_{\mathrm{ord}} + \Delta\alpha \tag{5}$$

Similarly, the state variables of the constant voltage controller are $x_{1\mathrm{i}}$ and U_{dcmi}, and the corresponding state space equation can be derived in the same form as (3)-(5), which is not described here.

2.2.3 PLL model. The control principle of the PLL at the rectifier station is equivalent to the structure block diagram shown in figure 5.

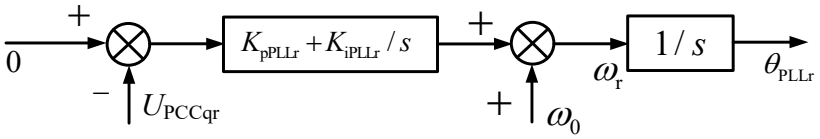

Figure 5. PLL model at the rectifier station.

The corresponding state space equation is shown in (6)

$$\begin{cases} \dfrac{\mathrm{d}\theta_{\mathrm{PLLr}}}{\mathrm{d}t} = \omega_{\mathrm{r}} \\ \dfrac{\mathrm{d}\omega_{\mathrm{r}}}{\mathrm{d}t} = -K_{\mathrm{pPLLr}} \dfrac{\mathrm{d}U_{\mathrm{PCCqr}}}{\mathrm{d}t} - K_{\mathrm{iPLLr}} U_{\mathrm{PCCqr}} \end{cases} \tag{6}$$

Where ω_{r} and θ_{PLLr} are the angular frequency and angle from the PLL. U_{pccqr} is the q-axis component of AC voltage of PCC (U_{pccr}). K_{pPLLr} and K_{iPLLr} are the proportion and the integral gain of the PLL. The state space equation of PLL model at the inverter station is similar to formula (6).

Additionally, the modeling method of AC system, DC transmission line, DC filter banks and AC filter banks has been described in detail in [7].

2.3. Small-signal dynamic model of LCC-HVDC system

By the linearization of the above state space model, the small signal model can be derived as

$$\frac{\mathrm{d}\Delta \boldsymbol{X}}{\mathrm{d}t} = \boldsymbol{A}\Delta\boldsymbol{X} + \boldsymbol{B}\Delta\boldsymbol{U} \tag{7}$$

In (7), $\boldsymbol{X}$ is the state variable vector, the input vector $\boldsymbol{U} = [I_{\mathrm{dcref}}, U_{\mathrm{dcref}}]^{\mathrm{T}}$, $\boldsymbol{A}$ is the state space matrix and $\boldsymbol{B}$ is the input matrix.

3 Small-signal model validation

In order to verify the validity of the small-signal model of LCC-HVDC system, the small-signal model is established in MATLAB while the detailed electromagnetic transient model is built in the PSCAD/EMTDC simulation platform.

3.1. Study parameters

The parameters of the main circuit and control system are shown in table 1 and table 2.

Table 1. The main parameters of LCC-HVDC.

The Group	Parameter Description	Value	
		Rectifier	Inverter
The rated value	DC current (kA)	3	
	DC voltage (kV)	500	
	AC voltage (kV)	525	525
The AC system	Short-circuit ratio	5.0	5.0

	Impedance angle	86.185°	85.23°
	PCC voltage (p.u.)	1.0	1.0
The transformer	Leakage reactor (p.u.)	0.16	0.152
	Capacity (MVA)	889.5	833.4
	Ratio of voltage	525/209.7	525/196.5
The PLL	Proportion gain	10	10
	Integral gain	50	50
The control system	Proportion gain	0.2	0.5
	Integral gain	100	50
	Time constant (s)	0.0012	0.02
The DC line	Inductor(H)	0.1979	0.1979
	Resistor(Ω)	5.2	5.2
	Capacitor(uF)	39	
	Smoothing inductor(H)	0.3	0.3

Table 2. The parameters of AC filter banks and DC filter banks.

The Group	Parameter Description		Value	
			Rectifier	Inverter
The DC filter banks	Capacitors (uF)	C_1	1.6	
		C_2	4.48	
		C_3	5.81	
	Inductors (mH)	L_1	10.869	
		L_2	10.384	
		L_3	20.6	
The AC filter banks (Type-A)	Capacitors (uF)	C_{1a}	1.605	1.963
		C_{2a}	56.824	3.709
	Inductors (mH)	L_{1a}	44.731	17.01
		L_{2a}	1.239	9.918
	Resistors (Ω)	R_{1a}	2500	500
The AC filter banks (Type-B)	Capacitors (uF)	C_{1b}	1.578	/
		C_{2b}	7.218	
		C_{3b}	7.704	
	Inductors (mH)	L_{1b}	8.116	
		L_{2b}	129.39	/
		L_{3b}	1.634	
	Resistors (Ω)	R_{1b}	400	/
		R_{2b}	1500	
The AC filter banks (Type-C)	Capacitors (uF)	C_{1c}	1.616	1.972
	Inductors (mH)	L_{1c}	2.721	3.964

It should be noted that the project parameters of the AC filter banks given in table 2 are for the bipolar system, so they need to be converted.

3.2. Model validation

This section compares the time-domain responses between the small-signal model and the detailed simulation in PSCAD/EMTDC. The system operates at nominal operation state originally (I_{dcref} =1.00 p.u., U_{dcref} =0.93 p.u). Figure 6 and figure 7 show the dynamic response of the measured DC-current I_{dcmr} and DC-voltage U_{dcmi} when the system is subjected to different step-changes.

The case in figure 6: U_{dcref} changes from 0.93 p.u. to 0.90 p.u. at time t=4s and recovers to 0.93 p.u. at time t=6s.

The case in figure 7: I_{dcref} changes from 1.00 p.u. to 0.95 p.u. at time t=10s and recovers to 1.00 p.u. at time t=12s.

It can be seen that the responses from the small-signal model are consistent with the simulation results from PSCAD/EMTDC, which verifies the accuracy of the small-signal dynamic model effectively.

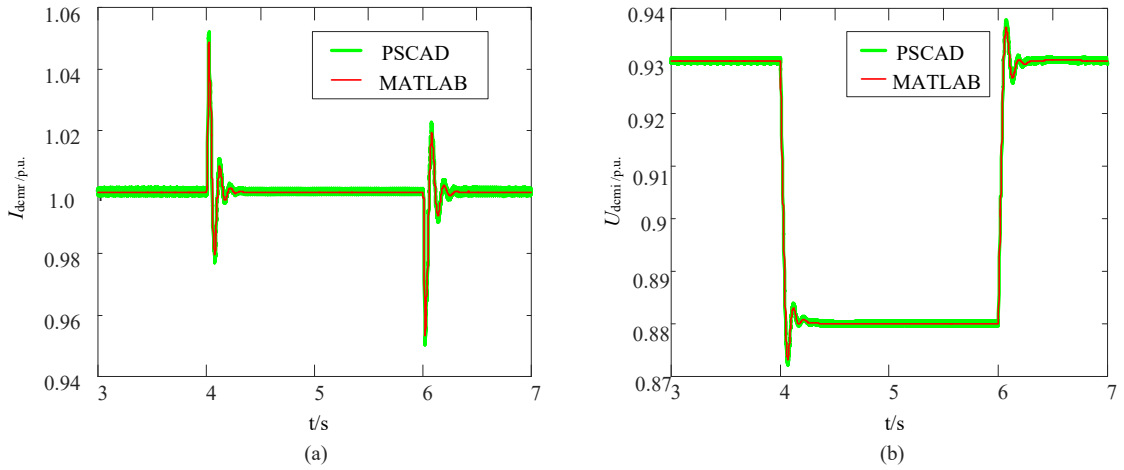

Figure 6. System dynamic responses under step-change of U_{dcref}.

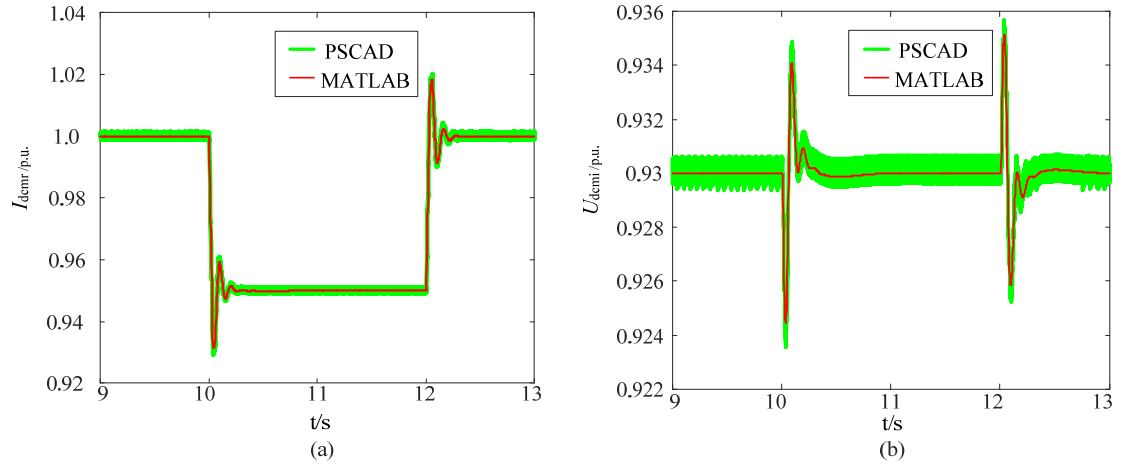

Figure 7. System dynamic responses under step-change of I_{dcref}.

4 Small-signal stability analysis

For the inverter station, commutation failure is more likely to occur in the case of weak AC grid. Based on this, this section mainly studies the influence of the inverter controllers on the oscillation mode, damping characteristics, participation factor and feasible stable operation region of the LCC system.

4.1. Impact of Proportional Gain (K_p) of Constant Voltage Controller

Initially, the system is in a stable operation state (on the rectifier side: SCR=5, V_{pcc_r}=1.00p.u, I_{dcref}=1.00p.u.; on the inverter side: SCR=2.5, V_{pcc_i}=1.00p.u., U_{dcref}=0.93p.u.). The control parameters are those of table 1. When the proportional gain K_p of the constant voltage controller varies from 0.1 to 4.1, the root loci of the eigenvalues are shown in figure 8 (a).

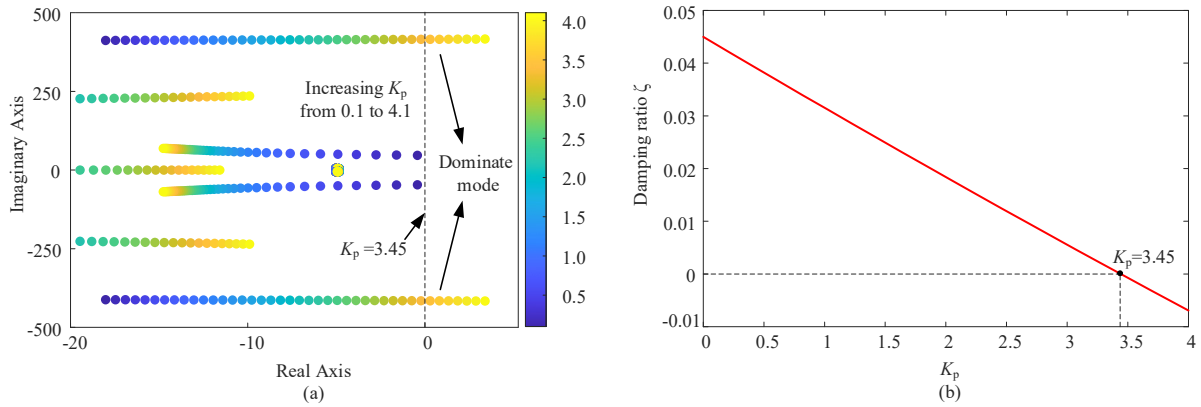

Figure 8. The eigen-analysis when K_p changes: (a) loci of the eigenvalues; (b) damping of dominant mode.

Figure 8 (a) shows that all the eigenvalues are in the left half plane when $K_p < 3.45$, indicating that the system can keep stable. It also can be observed that the stability margin decreases gradually with the increase of K_p. Figure 8 (b) depicts the damping ratio of the dominate mode when K_p changes. The result is that the damping of dominant mode decreases as K_p increases, and the small-signal stability is weakened correspondingly until the system becomes unstable at K_p =3.45.

In order to verify the correctness of the above conclusions more intuitively, K_p is step-changed from 0.5 to 4.1 at time t=4s and other parameters are kept unchanged in the PSCAD/EMTDC. The simulation result of the AC rms voltage is given in figure 9. It can be seen that the system becomes unstable when K_p is 4.1.

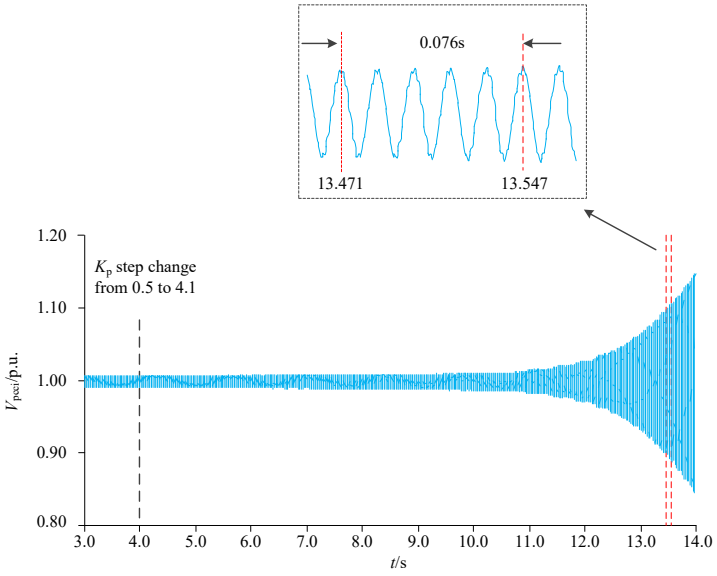

Figure 9. Dynamic response from PSCAD when K_p changes.

The oscillatory frequency of the dominant mode obtained from figure 9 is 65.79 Hz. Based on the analysis of the small-signal model established in MATLAB, the eigenvalues of dominant mode corresponding to the parameters in figure 9 are 3.393+*j*416.4 and 3.393-*j*416.4, which shows corresponding oscillation frequency of the system is 66.27Hz. This result is in agreement with simulation result, so the eigen-analysis of figure 8 is accurate.

Furthermore, the participation factor is used to analyze the relative participation of each state variable in regard to the dominant mode. The comparison of the normalized participation factor when K_p = 0.1 and K_p =4.1 is shown in figure 10.

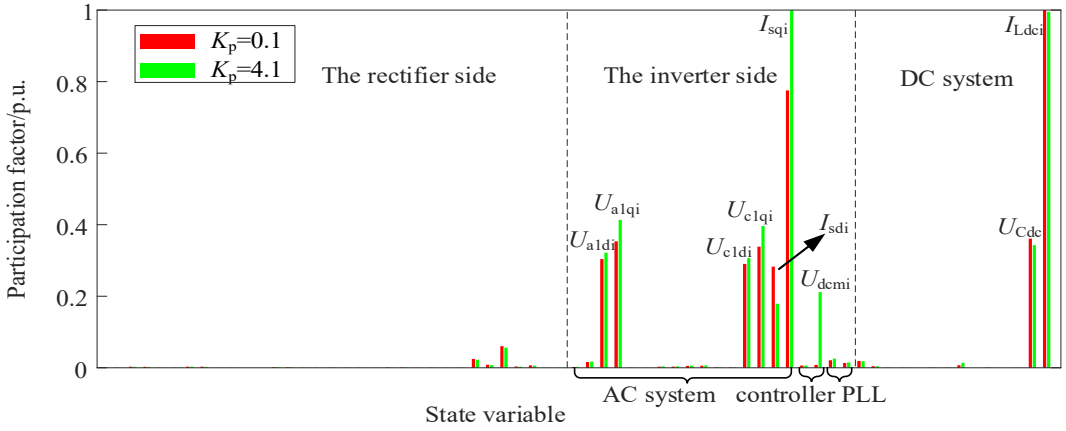

Figure 10. Participation factor of the state variables of dominant mode when K_p changes.

The participation factor of the state variable U_{dcmi} in the case of K_p =4.1 is significantly higher than that in the case of K_p =0.1, indicating that the main state variable making the system unstable is related to the constant voltage controller. Figure 10 also shows that the main state variables with relatively high participation factor remain unchanged as K_p changes greatly, that is to say, the impact of K_p on the dominant mode is not very prominent. Moreover, the main state variables that affect the mode are relevant to the AC system on the inverter side and the DC line, which suggests indirectly that the dominant mode is not closely related to the parameters K_p of the control system.

In this section, the feasible region of K_p which can keep the small-signal dynamic model stable is further studied as a function of SCR. The maximum acceptable values of

K_p are obtained when SCR varies from 2 to 3. Figure 11 shows the acceptable maximum value curve, below which is the feasible region of K_p. It can be found that the maximum allowable value of K_p decreases when the SCR increases under weak AC grid condition. In other words, the feasible value of K_p at lower SCR is not necessarily suitable for higher SCR, which may be contrary to normal cognition. Thus, the possible variation range of SCR should be considered when selecting the proportional gain K_p of constant voltage controller.

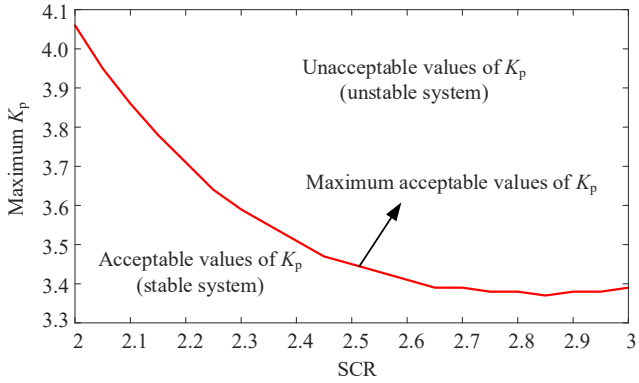

Figure 11. Acceptable values of K_p as a function of SCR

4.2. Impact of integral gain (K_i) of constant voltage controller

Initially, the system operates at stable operating point (on the rectifier side: SCR=5, V_{pcc_r}=1.00p.u, I_{dcref}=1.00p.u.; on the inverter side: SCR=2.5, V_{pcc_i}=1.00p.u., U_{dcref}=0.93p.u.). Figure 12 (a) shows the eigenvalue loci of the system when the integral gain K_i of the constant voltage controller varies from 30 to 100.

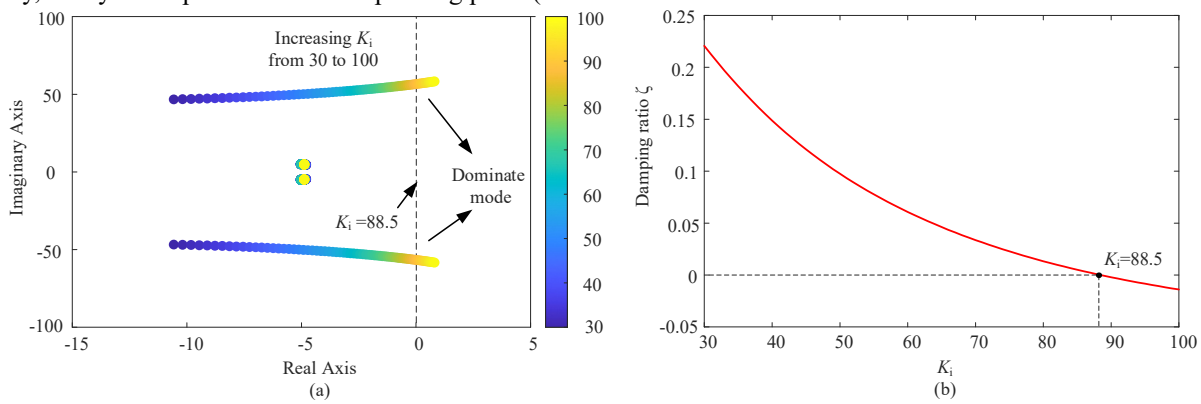

Figure 12. The eigen-analysis when K_i changes: (a) loci of the eigenvalues; (b) damping of dominant mode.

When K_i <88.5, all the eigenvalues of system always remain in the left-half plane, which suggests that the system can operate stably. In addition, with the increase of K_i, the stability margin of the system decreases and the small-signal stability is getting smaller. Curve of damping ratio of the dominant mode when K_i changes is shown in figure 12 (b). It is evident that the damping decreases with the increase of K_i. Figure 13 shows the dynamic response of the study system from PSCAD/EMTDC as K_i is step-changed from 30 to 100 at time t = 4.0 s. The observation from figure 13 indicates that the system can't keep stable when K_i =100.

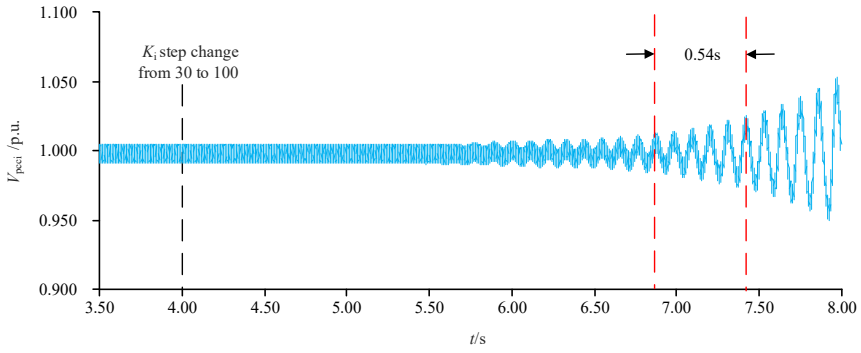

Figure 13. Dynamic response from PSCAD when K_i changes

Furthermore, based on the established small-signal model, the eigenvalues corresponding to the dominant mode are 0.8113+*j*58.30 and 0.8113-*j*58.30 when $K_i = 100$, whose oscillation frequency is 9.28Hz. The actual oscillation frequency from the simulation result in PSCAD is 9.26Hz. The similar result verifies the correctness of the above eigen-analysis.

The comparison of the normalized participation factor when K_i = 30 and K_i =100 is depicted in figure 14. The participation factor of state variables x_{1i} and U_{dcmi} become higher when K_i = 100 than that when K_i = 30, indicating the main state variables which lead to the instability of the system are related to the constant voltage controller. What's more, figure 14 shows that x_{1r} is also the main state variable affecting the dominant mode, so the dominant mode is closely relevant to the rectifier constant current controller.

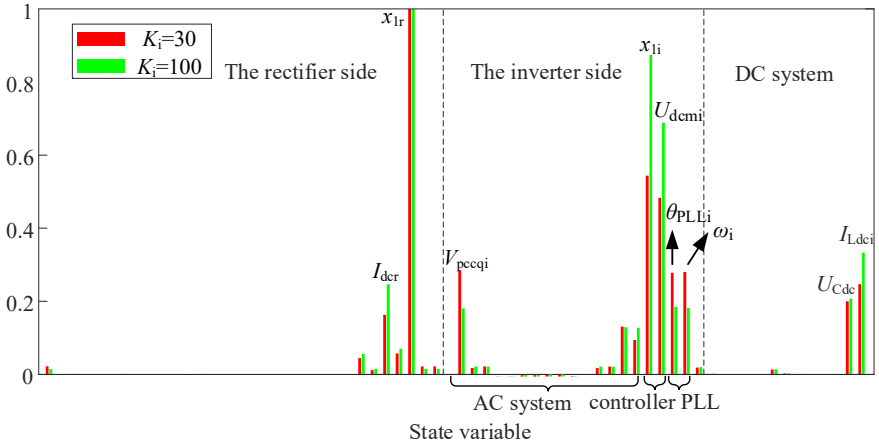

Figure 14. Participation factor of the state variables of dominant mode when K_i changes.

The impact of SCR on the inverter side, with the range of 2 to 3, is further studied here. By calculating the acceptable maximum of K_i which can make the system keep stable at every SCR value, the maximum allowable value curve can be obtained as figure 15. The feasible region of K_i is below the curve. It can be found that the critical value of K_i increases with the increase of SCR, in other words, increasing the SCR at the inverter station may improve the stability range of K_i. However, excessive K_i value will still lead to the system instability.

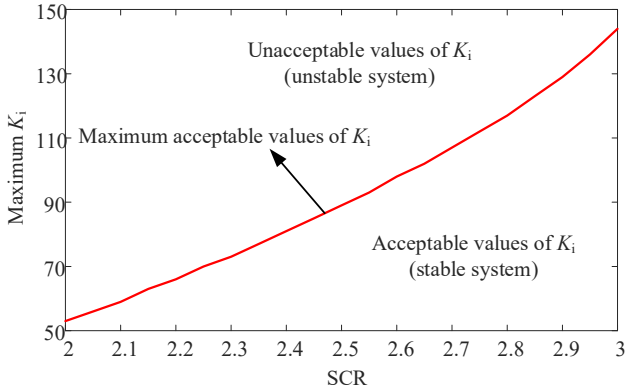

Figure 15. Acceptable values of K_i as a function of SCR.

5 Conclusions

This paper focuses on the influence of inverter controller parameters on the small-signal stability of LCC-HVDC system based on a practical project. By using the eigen-analysis method, the oscillation mode and damping characteristics of the LCC system can be obtained when controller parameters change. The corresponding conclusions are as follows:

1) Under weak AC grid condition (2 ≤ SCR ≤ 3), the small-signal stability of the system is weakened gradually with the increase of the proportional gain K_p of the constant voltage controller. At the same time, when SCR on the inverter side get larger, the maximum critical value of K_p becomes smaller. It should be noted that in order to ensure the stable operation of LCC-HVDC system, K_p need to be carefully selected according to the possible range of SCR.
2) As the integral gain K_i of the constant voltage controller increases, the small-signal stability of the system decreases gradually, and the maximum allowable value of K_i increases with the increase of SCR.

Acknowledgments

This work was financially supported by China Southern Power Grid Science and Technology Projects (ZBKJXM20190056).

References

1. Zhao W. (2011) HVDC technology. China Electric Power Press, Beijing.
2. Nayak, O.B., Gole, A.M., Chapman, D.G. (1994) Dynamic performance of static and synchronous compensators at an HVDC inverter bus in a very weak AC system. IEEE Transactions on Power Systems. 9, 3: 1350-1358.
3. Nayak, O.B., Gole, A.M., Chapman, D.G. (1995) Control sensitivity indices for stability analysis of HVDC systems. IEEE Transactions on Power Delivery. 10, 4: 2054-2060.
4. Jovcic, D., Pahalawaththa, N., Zavahir, M. (1999) Analytical modeling of HVDC-HVAC systems. IEEE Transactions on Power Delivery. 14, 2: 506-511.
5. Jovcic, D., Pahalawaththa, N., Zavahir, M. (1999) Small signal analysis of HVDC-HVAC interactions. IEEE Transactions on Power Delivery. 14, 2: 525-530.
6. Osauskas, C., Wood, A. (2003) Small-signal dynamic modeling of HVDC systems. IEEE Trans Power Del. 18, 1: 220-225.
7. Guo, C., Ning, L., Wang, H. (2017) Switching-function based dynamic model of LCC-HVDC station and small signal stability analysis. Power System Technology. 41, 12: 3862-3870.
8. Guo, C., Zhao, C., Iravani, R. (2017) Impact of phase-locked loop on small-signal dynamics of the line commutated converter-based high-voltage direct-current station. IET Generation, Transmission & Distribution. 11, 5: 1311-1318.
9. Chen, W., Ye, Y., Wang J. (2020) Influence of Constant Voltage Control and Predictive Constant Extinction Angle Control on Small-signal Stability of HVDC. Automation of Electric Power Systems. 44, 18: 98-106.
10. Zheng, A., Guo, C., Cui, P., Jiang, W., Zhao, C. (2019) Comparative Study on Small-Signal Stability of LCC-HVDC System With Different Control Strategies at the Inverter Station. IEEE Access. 7: 34946-34953.
11. Szechtman, M., Wess, T., Thio, C.V. (1991) A benchmark model for HVDC system studies. In: Proc.Int.Conf.AC DC Power Transmiss. pp: 374-378.